

Article

Microbial Mediated Synthesis of Silver Nanoparticles by *Lactobacillus plantarum* TA4 and Its Antibacterial and Antioxidant Activity

Hidayat Mohd Yusof ¹, Nor'Aini Abdul Rahman ^{1,2,*}, Rosfarizan Mohamad ^{1,2}
and Uswatun Hasanah Zaidan ³

¹ Department of Bioprocess Technology, Faculty of Biotechnology and Biomolecular Sciences, Universiti Putra Malaysia, Serdang 43400, Selangor, Malaysia; hidayatmy@gmail.com (H.M.Y.); farizan@upm.edu.my (R.M.)

² Bioprocessing and Biomanufacturing Research Centre, Faculty of Biotechnology and Biomolecular Sciences, Universiti Putra Malaysia, Serdang 43400, Selangor, Malaysia

³ Department of Biochemistry, Faculty of Biotechnology and Biomolecular Sciences, Universiti Putra Malaysia, Serdang 43400, Selangor, Malaysia; uswatun@upm.edu.my

* Correspondence: nor_aini@upm.edu.my; Tel.: +60-39-769-1945

Received: 18 August 2020; Accepted: 15 September 2020; Published: 5 October 2020



Abstract: The present study aimed to investigate the ability of *Lactobacillus plantarum* TA4 in tolerating Ag⁺ and its ability to produce silver nanoparticles (AgNPs). The biosynthesized AgNPs were characterized using UV–Visible spectroscopy (UV–Vis), dynamic light scattering (DLS), Fourier-transform infrared (FTIR), and high-resolution transmission electron microscope (HR-TEM). The cell biomass of *L. plantarum* TA4 demonstrated the ability to tolerate Ag⁺ at a concentration of 2 mM, followed by the formation of AgNPs. This was confirmed by the visual observation of color changes and a presence of maximum UV–Vis absorption centered at 429 nm. HR-TEM analysis revealed that the AgNPs were spherical with an average size of 14.0 ± 4.7 nm, while the SEM-EDX analysis detected that the particles were primarily located on the cell membrane of *L. plantarum* TA4. Further, DLS analysis revealed that the polydispersity index (PDI) value of biosynthesized AgNPs was 0.193, implying the monodispersed characteristic of NPs. Meanwhile, the FTIR study confirmed the involvement of functional groups from the cell biomass that involved in the reduction process. Moreover, biosynthesized AgNPs exhibited antibacterial activity against Gram-positive and Gram-negative pathogens in a concentration-dependent manner. Furthermore, the antioxidant property of biosynthesized AgNPs that was evaluated using the DPPH assay showed considerable antioxidant potential. Results from this study provide a sustainable and inexpensive method for the production of AgNPs.

Keywords: antibacterial; biosynthesis; FTIR; HR-TEM; *Lactobacillus*; silver nanoparticles; sustainable

1. Introduction

Silver nanoparticles (AgNPs) have been established in biomedical and biological applications as one of the promising nanoparticles due to their unique physical and chemical properties, including anticancer, drug delivery, and antimicrobial agents [1,2]. AgNPs have been reported to inhibit the growth of Gram-positive and Gram-negative pathogens [1]. The bactericidal properties of AgNPs may be attributed to the release of Ag⁺ [3], which is toxic to microorganisms. In this regard, AgNPs have been exploited as antimicrobial agents in wound dressing, topical cream [4], and food packaging [5]. Moreover, the unrestricted use of conventional antibiotics is a critical factor in the production of

resistance and the acquisition of drug resistance genes contributing to multidrug resistance [6]. Consequently, the use of AgNPs can potentially reduce the antibiotic resistance problem [7].

Over the last decade, the demand for sustainable alternatives to the conventional synthesis of AgNPs production has increased. The production of AgNPs is attained by physical and chemical methods that produce desirable size, shape, and better yield of NPs. Conventional methods, however, had significant drawbacks of high-cost production besides generating hazardous waste that causes environmental pollution. Therefore, it is imperative to look at other alternatives that are more sustainable and environmentally mild.

Generally, the NPs synthesis process employing biological entities such as microorganisms has received considerable attention as an alternative to conventional methods. Microorganism-mediated NP synthesis provides an eco-friendly, simple, low-cost approach that, most importantly, does not involve any hazardous chemical. Bacteria are vastly utilized in the synthesis of NPs because they are reproducible and considered a promising nanofactory for various kinds of NPs, including gold, zinc, silver, and selenium nanoparticles [8,9]. Certain bacteria possess unique cellular strategies for the production of NPs through the detoxification process of metal ion, mainly by metal ion biosorption and bioaccumulation [10]. Studies have confirmed that the ability of bacteria to produce NPs are highly dependent on their ability to resist the metallic ion. In particular, bacteria protect themselves from the harmful effects of metallic ion by reducing the ion into NPs with the aid of the cell membrane structure and biomolecules secreted by the cell [11,12]. The bacterial cell membrane is composed of numerous functional groups that act as a ligand for the metallic ion [13] and site for the formation of NPs. Some studies reported the isolation of metal-tolerant microorganisms from metal-rich ecological niches to synthesize NPs. Jain et al. [14] reported zinc-tolerant *Aspergillus aureus* NJP12 isolated from the zinc mine area demonstrated interactions between its metal resistance ability and its NPs synthesis potential. Likewise, the soil fungus *Cladosporium oxysporum* AJP03, which was isolated from a metal-rich district, exhibited gold metal tolerance and simultaneously produced gold nanoparticles [15]. Therefore, the ability of microorganisms to interact with metal ion enables them to act as the nanofactory of NPs.

Several studies have been conducted on the biosynthesis of AgNPs using lactic acid bacteria (LAB), particularly probiotic bacteria. LAB are Gram-positive non-pathogenic bacteria widely found in milk and fermented food products. This bacteria also exhibit health-promoting properties [16] for human and animal consumption. Studies also indicated LAB as a promising reducing agent for AgNPs production, e.g., Rajesh et al. [17] demonstrated that the supernatant of *Lactobacillus acidophilus* for AgNPs synthesis produced spherical-shaped particles size ranging from 4 to 50 nm. Likewise, numerous studies reported using LAB supernatant as a reducing agent for the synthesis of AgNPs [17–20]. Moreover, it was claimed that by manipulating the bacterial supernatant, the downstream processing during the AgNPs synthesis would become more straightforward and effortless [21]. However, the study using cell biomass from the LAB for the production of AgNPs is scant. Research into the ability of LAB cell biomass as a nanofactory may also shed some light on its potential application in decontamination and bioremediation applications.

In this present study, the biosynthesis of AgNPs was investigated using the cell biomass of probiotic *Lactobacillus plantarum* TA4. The probiotic strain was isolated from local fermented food ("tapai pulut") in our previous study, which demonstrated zinc-tolerant properties at a higher concentration and simultaneously developed zinc oxide nanoparticles (ZnO NPs) [10]. Therefore, based on our prior findings, here we demonstrate the potential of cell biomass of *L. plantarum* TA4 to interact with Ag^+ and its potential to produce AgNPs. The ability of *L. plantarum* TA4 to tolerate various Ag^+ concentrations were determined, and the formation of AgNPs was checked by UV-Visible spectroscopy. Later, the resulting AgNPs were characterized by dynamic light scattering (DLS), Fourier-transform infrared (FTIR), and high-resolution transmission electron microscope (HR-TEM). The biopotential applications such as antimicrobial and antioxidant activity were also investigated.

2. Materials and Methods

2.1. Materials

A 10 mM stock solution of silver nitrate (AgNO_3) was prepared by dissolving AgNO_3 in deionized water and was filter-sterilized using a disposable syringe filter (polyethersulfone membrane pore size 0.22 μm) (Whatman International, Maidstone, UK) before use. Zinc-tolerant probiotic *Lactobacillus plantarum* strain TA4, which was isolated from our previous work, was used for this study. The probiotic was cultivated in de Man, Rogosa, and Sharpe (MRS) (Oxoid™) medium. The composition of MRS broth are as follow (g/L); peptone, 10.0; Lab-Lemco powder, 8.0; yeast extract, 4.0; glucose, 20.0; dipotassium hydrogen phosphate, 2.0; sodium acetate, 5.0; triammonium citrate, 2.0; magnesium sulfate, 0.2; and manganese sulfate, 0.05. All reagents used were of analytical grade.

2.2. Bacterial Culture and Biomass Extraction

L. plantarum strain TA4 was grown overnight in the 100 mL of MRS medium and incubated at 37 °C with 150 rpm agitation. After incubation, biomass was harvested by centrifugation (2800× g for 10 min), and the supernatant was discarded. The collected biomass was washed thrice with phosphate-buffered saline (PBS), and the obtained biomass was used for the biosynthesis of AgNPs.

2.3. Determination of Maximum Tolerable Concentration (MTC) against Ag^+

To determine the maximum tolerable concentration (MTC) value of *L. plantarum* TA4 towards silver ion, method described by Presentato et al. [22] was followed with some modification. About 2 g of wet biomass of the strain TA4 (1.2×10^6 colony forming unit per mL (CFU/mL)) was suspended in 100 mL aqueous solution of silver ion (Ag^+). The bacterial cell was exposed with an increasing concentration of Ag^+ (1, 2, 4, 6, 8, and 10 mM) to assess the *L. plantarum* TA4's silver-tolerance potential. The suspension was incubated overnight at 37 °C, and the cell viability was determined by a spot plating technique. In brief, the bacterial suspension was serially diluted and then was spotted onto MRS agar plate for each of the tubes. The MTC was defined as the maximum concentration of Ag^+ inhibiting the growth of bacteria. The experiments were performed in triplicates. The MTC result was used for the biosynthesis process in the subsequent study.

2.4. Biosynthesis of Silver Nanoparticles (AgNPs) Using *L. plantarum* TA4

The biosynthesis of AgNPs was performed following the method described by Thomas et al. [23] and Markus et al. [9] with some modifications. About 2 g of wet biomass of the strain TA4 was suspended in 100 mL of sterilized deionized water containing 2 mM of Ag^+ concentration. The suspension was then incubated at 37 °C for 24 h with an agitation of 150 rpm in the dark. After the incubation time, the resulting dark brown solution was centrifuged at high speed (18000× g for 30 min) to collect the biomass and biosynthesized AgNPs. The dark brown, collected biomass was washed with buffer and resuspended in sterilized deionized water. To obtain the biosynthesized AgNPs, the suspension was subjected to ultrasonication cycles to disrupt the biomass cell and centrifuged (2800× g for 15 min) to obtain the AgNPs that were dispersed in the suspension (the pellet was discarded). For the antibacterial and antioxidant assessment, the colloidal form of biosynthesized AgNPs was subjected to freeze-drying to obtain a dry powder form. Figure 1 shows the biosynthesis process, characterization, and assessment for biopotential applications of AgNPs.

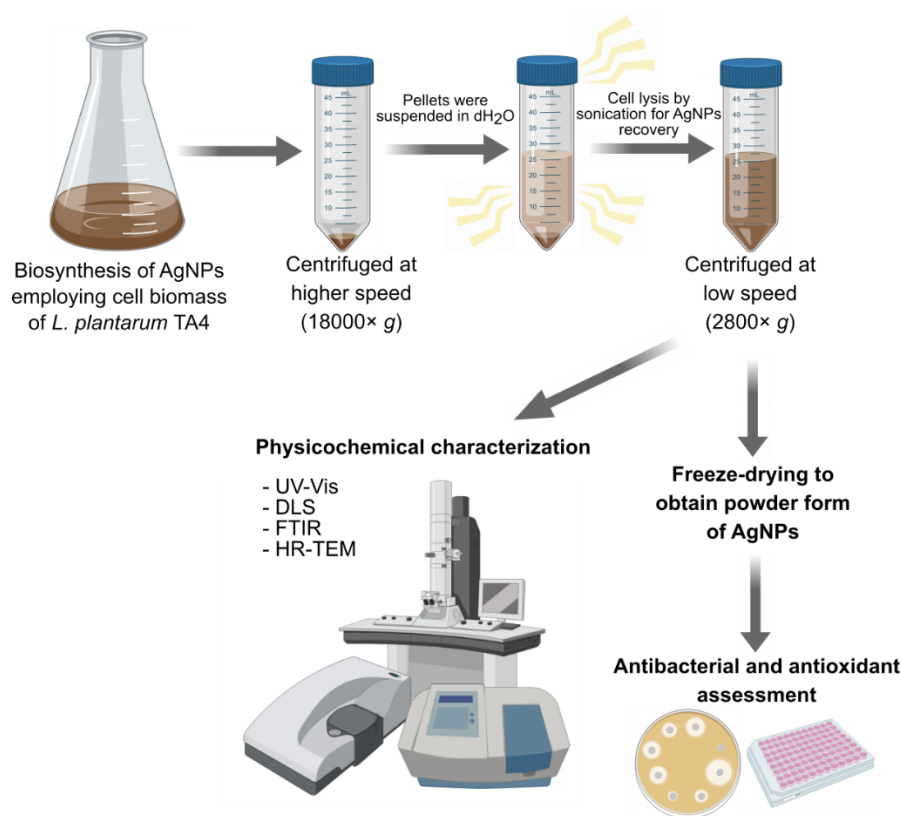


Figure 1. Schematic representation for biosynthesis, characterization, and biopotential applications of biosynthesized silver nanoparticles (AgNPs).

2.5. Characterization of Biosynthesized AgNPs

The reduction of Ag^+ to AgNPs in the aqueous solution was monitored using a UV–Visible spectroscopy (Uviline 9400, Secomam, Alès, France) within the range of 300 to 600 nm. The UV–Visible spectra of AgNO_3 solution (1 mM) without cell biomass was used as control. The presence of functional groups on AgNPs was determined by Fourier-transform infrared spectra (FTIR) in the range of 4000 to 400 cm^{-1} at a resolution of 4 cm^{-1} using Nicolet 6700 (Thermo Fisher Scientific, Madison, US), and the transmittance spectrum was recorded. The colloidal solution of AgNPs and dried cell biomass of *L. plantarum* TA4 (control) were used for the analysis. The hydrodynamic size and polydispersity index (PDI) of biosynthesized AgNPs were determined by dynamic light scattering (DLS) using a Nano S (Malvern Instruments, Malvern, UK). Briefly, the colloidal solution of AgNPs in cuvettes was measured, and the values were generated using the software equipped with the instrument. The morphology and size of biosynthesized AgNPs were analyzed using a high-resolution transmission electron microscope (HR-TEM). A drop of AgNPs sample was placed on a copper grid and air-dried before viewing using JEM-2100F (Jeol, Tokyo, Japan). The particle size distribution of biosynthesized AgNPs was measured using the ImageJ version 2.0 software (NIH).

2.6. Scanning Electron Microscope (SEM) and Energy Dispersive X-ray (EDX) of *L. plantarum* TA4 Exposed to Ag^+

SEM-EDX analysis was performed to investigate the formation of AgNPs on the cell membrane of *L. plantarum* TA4. Briefly, strain TA4 was grown overnight in MRS broth at $37\text{ }^\circ\text{C}$, and the cell biomass was collected by centrifugation at $2800\times g$ for 10 min. The collected cell biomass was washed with phosphate-buffered saline (PBS) three times. Subsequently, the cell biomass was added to the Ag^+ aqueous solution at a concentration of 2 mM and incubated in the dark at $37\text{ }^\circ\text{C}$ for 24 h. The color change at the end of the incubation time indicated the formation of AgNPs, and the cell biomass

was collected by centrifugation and washed according to the described procedure. The biomass was subjected to sample processing for SEM. In brief, the cells were fixed in 2.5% glutaraldehyde for 4 h at 4 °C and washed thrice with 0.1 M sodium cacodylate buffer before being post-fixed with 1% osmium tetroxide for 2 h at 4 °C. Afterwards, the cells were washed again with the buffer and dehydrated with graded acetone series (35, 50, 75, 95, and 100% with 10 min per step). The dehydrated cell was then subjected to critical point-dried before mounted on the stub and coated with gold film in the sputter coater. The SEM observation was performed using JEOL JSM-6400 equipped with an EDX spectrometer. The EDX analysis was used to determine the elemental silver present on the cell membrane.

2.7. Antibacterial Assay of Biosynthesized AgNPs

The antibacterial assessment of biosynthesized AgNPs was performed by agar well diffusion method against Gram-positive (*Staphylococcus aureus* and *Staphylococcus epidermidis*) and Gram-negative (*Escherichia coli* and *Salmonella* sp.) pathogens. The powder form of biosynthesized AgNPs was suspended in sterilized deionized water before use. The inoculum of each pathogen was grown overnight in nutrient broth at 37 °C. Sterilized swabs were used to streak each pathogen onto the nutrient agar. Simultaneously, wells were punched with sterile borer and about 100 µL of biosynthesized AgNPs at different concentrations (12.5, 25, 50, 100, and 200 µg/mL) were added to each well. The plate was incubated at 37 °C for 24 h, and the diameter of the inhibition zone was measured. The experiment was performed in triplicates.

2.8. Antioxidant Activity of Biosynthesized AgNPs

The antioxidant activity of biosynthesized AgNPs was determined by 2,2-diphenyl-1-picrylhydrazyl (DPPH) free radical scavenging assay (RSA) according to the method of Safawo et al. [24] with some modification. Briefly, 1 mL of 0.1 mM DPPH (3.94 mg dissolved in 100 mL methanol) was added to 1 mL aliquot of different concentration (31.3, 62.5, 125, 250, 500, and 1000 µg/mL dispersed in methanol) of biosynthesized AgNPs. The mixture was vortexed thoroughly and incubated in the dark for 30 min. The absorbance was recorded at 517 nm using a UV–Visible spectroscopy (Uviline 9400, Secomam, Alès, France) at the end of the incubation. DPPH without sample was used as the control, and methanol was used as the blank. The same procedure was carried out using ascorbic acid as a standard antioxidant. The percentage of DPPH scavenging activity was calculated by the following formula:

$$RSA_{DPPH} = \frac{A_{control} - A_{test}}{A_{control}} \times 100$$

2.9. Statistical Analysis

Data from antioxidant activity were analyzed by one-way analysis of variance (ANOVA) and the comparison between groups was performed using Tukey's test to determine statistical significance. Statistical analysis was performed using Graphpad Prism version 7.0 software (La Jolla, California, USA). The significance was set at $p < 0.05$.

3. Results and Discussion

3.1. Maximum Tolerable Concentration (MTC) of *L. plantarum* TA4 against Ag^+

The research on the use of bacteria for the biosynthesis of NPs has gained considerable attention in the last decade as an alternative to the conventional method. In general, not all bacteria can synthesize NPs. The synthesis of NPs depends on the ability of bacteria to resist the metal ion, where the bacteria tend to reduce the ion into respective NPs metal [25] under the metal stress. Some bacteria have been documented to tolerate metal ion and have the potential for metal NPs synthesis [10,14,22,26,27]. In our study, the cell biomass of *L. plantarum* TA4 demonstrated a MTC against Ag^+ at 4 mM (based on

cell growth). Moreover, no growth was observed beyond the MTC value, indicating the toxic effect of Ag^+ to the cell (Figure 2a).

Further, the formation of AgNPs was confirmed using UV–Visible spectroscopy. The reduction of Ag^+ into AgNPs was evaluated by recording the absorption spectrum of the reaction. UV–Visible spectra show no evidence of absorption in the range of 400 to 500 nm for the control suggests the absence of AgNPs. As presented in Figure 2b, a narrow absorption spectrum with a main band centered at 429 nm was obtained at a concentration of 2 mM, which corresponds to surface plasmon resonance (SPR) of AgNPs. Moreover, a broad absorption spectrum was observed at concentrations of 1, 4, 6, 8, and 10 mM with main bands centered at 441, 410, 335, 406, and 407 nm, respectively, which implies the formation of AgNPs. The results show that the SPR band intensity increased as the AgNO_3 concentration increased from 1 mM to 2 mM and the band intensity began to decrease above this concentration (at concentration of 4, 6, 8, and 10 mM). The possible reason for this may be due to the toxic effect of high Ag^+ concentration on cells that restricting the formation of NPs, resulting in only a limited amount of AgNPs produced (based on gradually changes of color from dark brown to transparent color). Furthermore, this behavior correlates with no viable cells (Figure 2a) obtained beyond 4 mM. Meanwhile, a broad absorption spectrum was obtained at Ag^+ concentration of 1 mM compared to 2 mM which may be attributed to lower availability of Ag^+ to react with the cells, resulting in less AgNPs production and consequently generating wider spectrum. However, the SPR band intensity was found to be higher at a concentration of 2 mM probably because the cells were able to tolerate with Ag^+ and more AgNPs were produced resulting in increased band intensity.

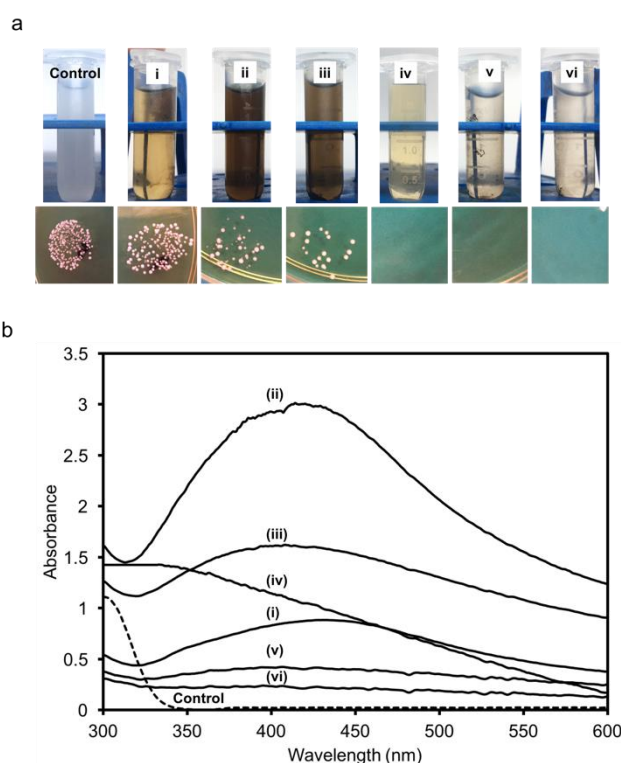


Figure 2. (a) Maximum tolerable concentration of *L. plantarum* TA4 exposed to increasing concentration of Ag^+ . The bacterial cell growth was determined by the spot plating technique. (b) UV–Visible absorption spectra of biosynthesized AgNPs by *L. plantarum* TA4 exposed with different concentrations of Ag^+ . (Control) AgNO_3 , (i) 1 mM, (ii) 2 mM, (iii) 4 mM, (iv) 6 mM, (v) 8 mM and (vi) 10 mM.

It is clear that *L. plantarum* TA4's capability to produce AgNPs depends on its ability to resist Ag^+ . Likewise, *Bacillus* strain CS11, which was isolated from heavy metal contamination areas, can form AgNPs when treated with 1 mM Ag^+ [21]. Presentato et al. [22] also reported *Rhodococcus aetherivorans*

BCP1 as having the ability to detoxify selenium ion at higher concentration and simultaneously produced selenium NPs. Nevertheless, *L. plantarum* TA4 exhibited lower resistance to Ag^+ compared to other reported microorganisms [28]. Several studies have been done in the isolation of metal tolerance-microorganisms from ecological niches rich in metal for the synthesis of NPs [14,15]. In our study, *L. plantarum* TA4 was isolated from local fermented food, which explained its low resistance to Ag^+ . Further, based on the above explanation, it was suggested that the metal resistant ability of microorganisms is also depending on the species because each species has different metabolic process and defense mechanism related to their biochemical pathway to withstand such toxicity [25,29,30]. In this study, the *L. plantarum* TA4 demonstrated MTC value at 4 mM and showed a pronounced spectrum at a concentration of 2 mM. Hence, the Ag^+ concentration at 2 mM was chosen for the synthesis of AgNPs in the subsequent study.

3.2. Biosynthesis of AgNPs Using *L. plantarum* TA4 Biomass

For the biosynthesis of AgNPs, the aforesaid method was performed. Similarly, the reduction of Ag^+ to AgNPs was determined by visual observation correlated with color change. Figure 3a displays the reaction mixture of *L. plantarum* TA4 cell biomass in the Ag^+ suspension (white) that turned dark brown after 24 h of incubation, suggesting the formation of AgNPs. It is well known that the color change is due to the excitation of SPR of the AgNPs. The UV–Visible absorption spectra analysis presented in Figure 3b revealed the maximum SPR excitation band of biosynthesized AgNPs centered at 429 nm, which is the typical peak obtained for AgNPs. The maximum absorption band obtained in this study is similar to the range reported in other studies [31,32].

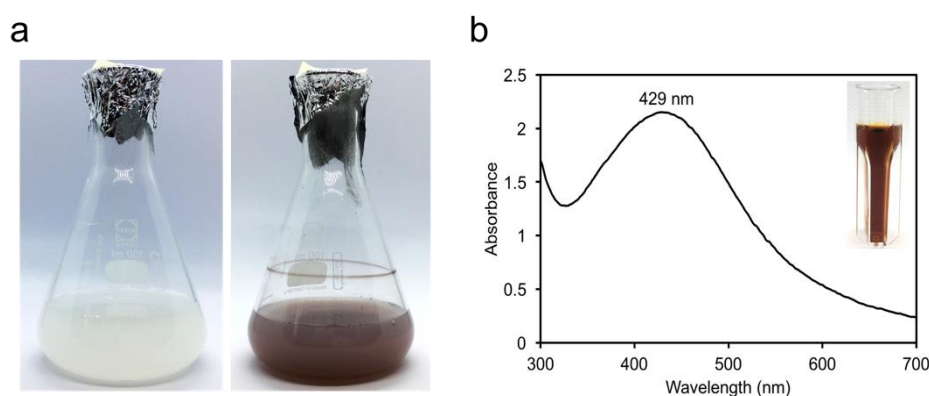


Figure 3. (a) Visual observation of AgNPs formation by cell biomass of *L. plantarum* TA4. (b) UV–Visible absorption spectra of biosynthesized AgNPs. The inset image shows the visual observation of biosynthesized AgNPs.

While several studies have been conducted on the biosynthesis of AgNPs using a microbial source, a critical aspect to the development of a safe and non-pathogenic microbial platform is still lacking. A previous study by El-Shanshoury et al. [33] utilized the supernatant of *E. coli* for the synthesis of AgNPs. Likewise, Nanda and Saravanan [34] produced AgNPs with the culture supernatant of *S. aureus*. Both bacteria are recognized as common opportunistic pathogens that may pose safety issues during the AgNPs synthesis process. Therefore, this study exploited beneficial bacteria, *L. plantarum* TA4, in the production of AgNPs to overcome the problems that may arise when using pathogenic organisms. *Lactobacillus* is of particular interest due to its non-pathogenic feature and food-grade status, i.e., the “generally recognized as safe” (GRAS) bacteria confirmed not to exhibit any adverse effects on the individual handling it [25]. Microorganisms exhibit an inherent potential to synthesize AgNPs through either the culture supernatant or the cell biomass route. In contrast, several studies documented the biosynthesis process using culture supernatant, and fewer studies used the cell biomass of *Lactobacillus*. Microorganism-mediated synthesis of AgNPs employing *Lactobacillus* through

various routes is presented in Table 1. It should be noted that biosynthesis using culture supernatant involved a nutrient in the culture medium that might facilitate the formation of AgNPs; hence, the exact identification of biomolecules involved in the synthesis process using culture supernatant is still uncertain. Nevertheless, in this study, we solely use cell biomass of *L. plantarum* TA4 for the biosynthesis process, which denotes the capability of the microorganism to synthesize AgNPs. Moreover, the AgNPs generated in this study are smaller than the other reported studies (Table 1) using the *Lactobacillus* species and on par with the route using cell culture supernatant, which underlines the significance of our finding.

Table 1. *Lactobacillus* mediated synthesis of silver nanoparticles.

Species	Route	Size (nm)	Reference
<i>Lactobacillus</i> sp.	Supernatant	30–100	[19]
<i>Lactobacillus acidophilus</i>	Cell biomass	30	[35]
<i>Lactobacillus plantarum</i>	Cell biomass	33.4	[35]
<i>L. acidophilus</i>	Supernatant	4–50	[17]
<i>Lactobacillus delbrueckii</i>	Supernatant	54–113	[36]
<i>Lactobacillus</i> sp.	Supernatant	14	[37]
<i>Lactobacillus mindensis</i>	Supernatant	20	[38]

Earlier studies indicated that the fundamental mechanisms for the formation of AgNPs were facilitated by the enzyme nitrate reductase [7,39], which involved the transfer of electrons from nitrate to the metal group [40]. Likewise, Wang et al. [41] reported that the reduction of selenium nanoparticles by *Proteus mirabilis* YC801 occurred by cytoplasmic enzymatic reduction involving thioredoxin reductase, glutathione reductase, or NADH-related reductase. On the other hand, Sintubin et al. [11] discovered the biosynthesis of AgNPs through the interaction of Ag⁺ with the functional groups present on the cell membrane of several *Lactobacillus* species. The AgNPs were observed to be distributed on the outer layer of the bacterial cell, as visualized by TEM [11]. As a Gram-positive bacteria, *Lactobacillus* is composed of a thick layer of peptidoglycan, polysaccharides, teichoic acids, and proteins that provide many anionic surface groups on the cell membrane [10,42]. When the cells are exposed to Ag⁺, the silver cation will bind to the anionic surface, providing sites for the biosorption [11]. At this point, Ag⁺ interacts with proteins and other functional groups of the cell that serve as an electron donor by reducing Ag⁺ to its respective metal atom (Ag⁰) and subsequently developing AgNPs. Moreover, proteins may also bind to AgNPs through free amino or carboxyl groups, which serve as capping agents [43]. Therefore, it can be postulated that biomolecules and functional groups present in bacterial cells or secreted by the bacteria serve as the reducing agents and promote the production of AgNPs. To sum up, the cell biomass of *L. plantarum* TA4 has demonstrated the potential as a nanofactory for the development of AgNPs without the use of harsh chemicals and high energy consumption. Subsequently, the formation of AgNPs was validated by FTIR analysis to determine the functional groups involved in the synthesis process.

3.3. Dynamic Light Scattering (DLS) Analysis

The hydrodynamic size and PDI of the biosynthesized AgNPs were investigated by DLS analysis in a colloidal solution. The average AgNPs size obtained is 74 ± 39 nm, with a PDI value of 0.193 (Figure 4), indicating the monodispersed nature of the formed AgNPs. DLS is one of the most commonly used techniques to measure the size characterization of NPs. Nevertheless, hydrodynamic size measurements obtained through DLS were not only conducted on the metallic core, but also with all substances that bind or covered the surface of NPs [44], which resulted in a bigger NPs sizes. Further explanation of the size characterization of AgNPs was discussed in the HR-TEM study.

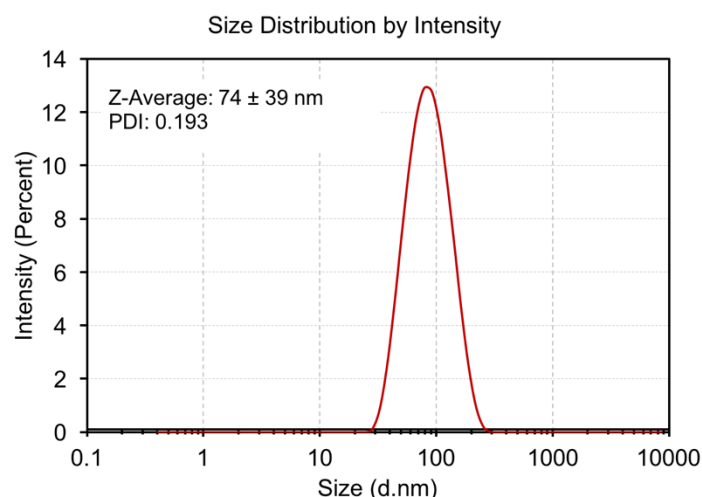


Figure 4. Size distribution of biosynthesized AgNPs by dynamic light scattering (DLS) analysis.

3.4. FTIR Analysis

The FTIR spectra provide information of functional group or biomolecules on the surface of the biosynthesized AgNPs. In the present study, FTIR analysis was performed to identify the potential functional group in *L. plantarum* TA4 which responsible in the reduction and stabilization of AgNPs. The obtained FTIR spectrum is shown in Figure 5. Several intense bands are observed on the biosynthesized AgNPs at 3197, 2924, 1634, 1518, 1450, 1209, 1030, and 961 cm^{-1} (Table 2), whereas the cell biomass of *L. plantarum* TA4 showed intense bands at 3254, 1636, 1551, 1456, 1224, 1078, and 994 cm^{-1} . The bands obtained from the cell biomass of *L. plantarum* TA4 were used as references, where the functional group was involved in the synthesis and stabilization process. A broad band located at 3197 cm^{-1} (was shifted from 3254 cm^{-1} in cell biomass) can be assigned to the stretching vibration of hydroxyl group ($-\text{OH}$) and amine group ($\text{N}-\text{H}$ stretching vibration in primary and secondary amines of amino acids, peptides and proteins) [45] implied their involvement in the synthesis of AgNPs. The band at 2924 cm^{-1} corresponds to the $\text{C}-\text{H}$ stretching vibration which not observed in the cell biomass, and the band at 1634 cm^{-1} could be attributed to $\text{C}=\text{O}$ stretching of Amide I in addition to peptide bond which may involve in the stabilization of AgNPs as reported by Hamouda et al. [45]. Meanwhile, the intense band at 1518 cm^{-1} corresponds to Amide II ($\text{N}-\text{H}_2$ deformation in primary amide and $\text{N}-\text{H}$ bending and $\text{C}-\text{N}$ stretching in secondary amide). The band at 1450 cm^{-1} could be assigned to $\text{C}-\text{H}$ bending mode of methyl and methylene group in protein and same band was also observed in the cell biomass. Concurrently, the band of 1209 cm^{-1} in AgNPs (which was shifted from 1224 cm^{-1} in cell biomass) corresponds to $\text{C}-\text{N}$ stretching and PO_2^- asymmetric stretching. Moreover, the band observed at 1030 cm^{-1} in AgNPs can be assigned to $\text{C}-\text{O}$ stretching of carboxyl group, which was shifted from 1078 cm^{-1} in cell biomass. Lastly, the small band (994 cm^{-1} in cell biomass) shifted toward a lower wave number was observed at 961 cm^{-1} , which can be assigned to the bending vibration of $\text{C}=\text{C}$ group. In this study, the obtained functional groups on biosynthesized AgNPs (hydroxyl, protein, and carboxyl) verified the presence of biomolecules from the cell membrane of *L. plantarum* TA4, which was involved in the biosynthesis process.

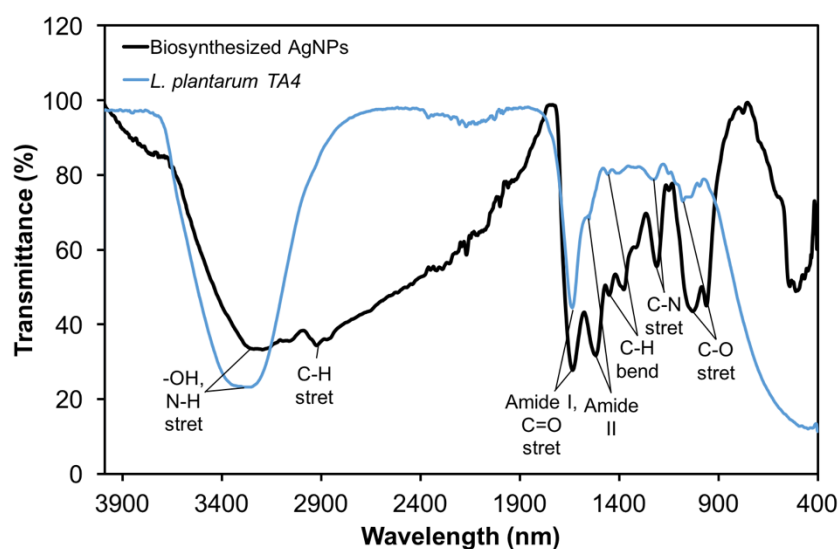


Figure 5. FTIR spectrum of the *L. plantarum* TA4 biomass (blue line) and the biosynthesized AgNPs (black line).

Table 2. Main spectra bands and functional groups interpretation of *L. plantarum* TA4 and biosynthesized AgNPs.

Spectra Band (cm ⁻¹)		Functional Group and Vibrational Assignment
<i>L. plantarum</i> TA4	Biosynthesized AgNPs	
3254	3197	Hydroxyl group (-OH)/amide group (N-H stretching vibration)
	2924	C-H stretching vibration
1636	1634	Amide I (C=O stretching vibration)
1151	1518	Amide II
1456	1450	C-H bending vibration
1224	1209	C-N stretching vibration, PO ₂ - asymmetric stretching
1078	1030	C-O stretching vibration
994	961	C=C bending vibration

3.5. SEM-EDX and HR-TEM Analysis

SEM-EDX analysis was carried out to reveal the formation of biosynthesized AgNPs by the cell biomass of *L. plantarum* TA4. Figure 6b shows the formation of particles outside the cell (indicated by the yellow arrow) compared to the control (Figure 6a). From the result, the formation of AgNPs occurred on the cell membrane of *L. plantarum* TA4. However, only a few particles are observed in Figure 6b which may be due to the effect of sample processing resulting in some particles washed away. From our previous study, we suggested that the functional groups and protein present on the cell membrane of *L. plantarum* TA4 facilitated the formation of NPs by serving as a binding site for metal ion before the development of NPs [10]. In our current study, a similar finding was reported, and this validated that the formation of metal NPs by *L. plantarum* TA4 cell was through the involvement of cell membrane. A similar observation was reported by Moreno-Martin et al. [46] employing *L. reuteri* in the biosynthesis of selenium NPs, which took place on the cell membrane. Additionally, they also reported that the formation of NPs was initiated by the exopolymeric substance (EPS) secreted by the bacteria. In this study, the extracellular formation of AgNPs was confirmed by EDX spectra, which revealed an elemental silver peak implying the presence of AgNPs (Figure 6c). Moreover, the observed other element peak signals by EDX spectra is due to the chemical used for sample processing and coating process with gold film. Overall, our findings suggested that the formation of AgNPs was facilitated by

the functional group present on the cell membrane of *L. plantarum* TA4, which also corresponded to our FTIR results and other studies [35,46,47].

HR-TEM was performed to investigate the morphology and size distribution of biosynthesized AgNPs. Figure 6e,f indicate that the particles are predominantly spherical with an average particle size distribution ranging from 4.7 to 24.3 nm (Figure 6d), with an average size of 14.0 ± 4.7 nm. Moreover, the biosynthesized AgNPs were well dispersed without significant agglomeration. The average size obtained by TEM contradicted with the average size obtained using the DLS analysis, whereby a bigger size of AgNPs was documented in the latter.

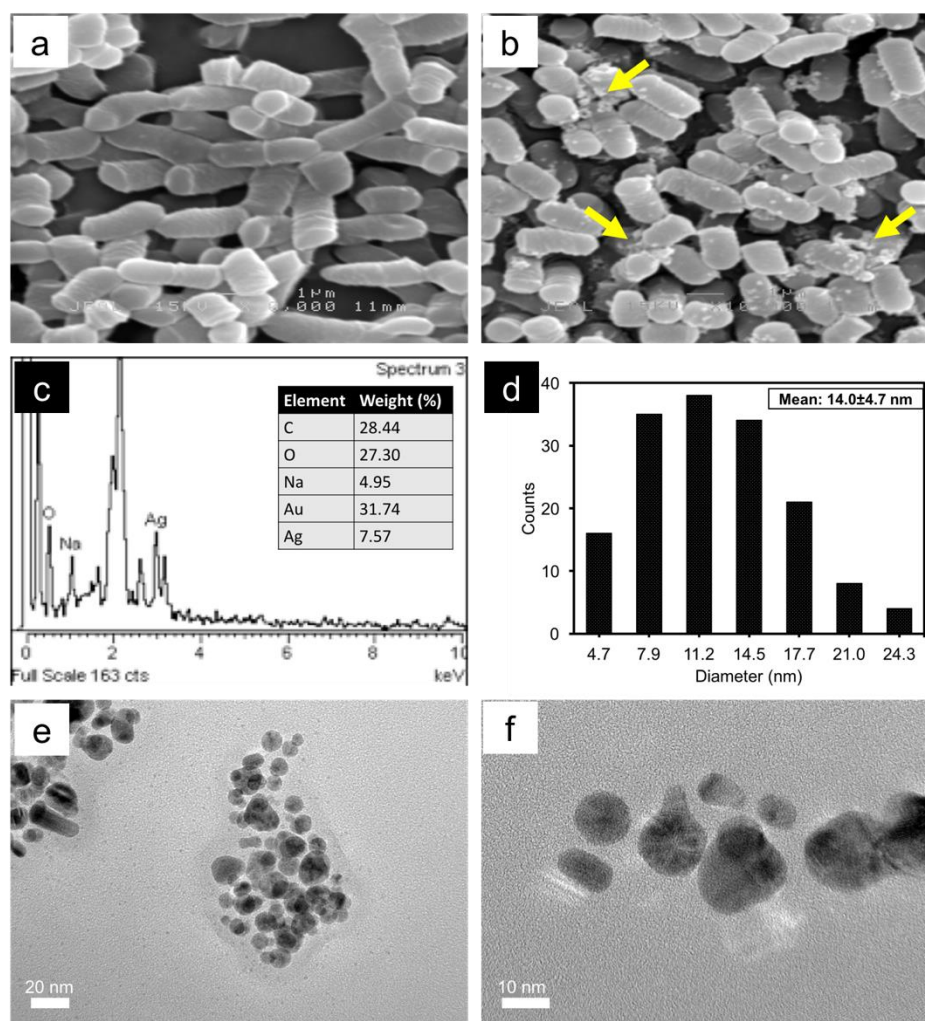


Figure 6. Scanning electron microscope (SEM) micrograph of *L. plantarum* TA4 (a) unexposed to Ag^+ (b) exposed to Ag^+ . SEM scale bar = 1 μm . (c) Energy dispersive X-ray (EDX) spectra of *L. plantarum* TA4 exposed to Ag^+ . (d) The particles size distribution of biosynthesized AgNPs. (e) High-resolution transmission electron microscope (HR-TEM) micrographs of biosynthesized AgNPs at scale bar = 20 nm. (f) HR-TEM micrographs of biosynthesized AgNPs at scale bar = 10 nm.

Our DLS result showed that the average hydrodynamic size was approximately 70% (74 nm) higher than the size obtained using TEM. The difference in size obtained between DLS and TEM may be due to several factors. Technically, the DLS measurement analysis is mainly based upon the intensity of light scattered by NPs in the solutions. In this context, the average size obtained is the intensity-weighted mean diameter from the cumulants analysis, in which larger NPs may be weighted significantly compared to smaller NPs [48]. Furthermore, our FTIR results detected the presence of protein and other functional groups from strain TA4 on the surfaces of AgNPs. In this sense,

the attachment of these organic molecules that encapsulated the NPs led to the increased NPs sizes. Moreover, the measurement of hydrodynamic diameter was calculated from the core of the NPs to the water shell that surrounds the NPs [44,48], while TEM analysis only measures the core of the NPs. Lastly, it was speculated that the significant increase in size might be attributed to the agglomeration of AgNPs in the suspension. Gosens et al. [49] reported that the size of NPs was increased up to four times when suspended in PBS due to the agglomeration of NPs. The resulting agglomeration state was affected by the pH and ionic strength of the aqueous suspensions, which subsequently led to the accumulation of NPs by weak van der Waals forces and the formation of large-size NPs in the DLS [49]. Nevertheless, the agglomeration of NPs is a reversible condition; it can be disrupted by the ultrasonication process. In our study, the suspension of AgNPs was not subjected to the ultrasonication process before the DLS analysis, which may have led to a significant increase in size through the agglomeration of AgNPs.

3.6. Antibacterial Activity of Biosynthesized AgNPs

The antibacterial activity of biosynthesized AgNPs was carried out using the agar well diffusion method (Figure 7a) against Gram-positive (*S. aureus* and *S. epidermidis*) and Gram-negative (*E. coli* and *Salmonella* sp.) pathogens employing various concentrations of AgNPs (12.5, 25, 50, 100, and 200 $\mu\text{g/mL}$). Figure 7b depicts the increased inhibition zone associated with the increase of AgNPs concentration, which may be due to more Ag^+ being released at a higher concentration. It was found that the inhibitory effects of AgNPs against all tested pathogens were similar. Previous studies reported that the inhibitory effect of AgNPs was more pronounced on Gram-negative bacteria compared to Gram-positive bacteria due to the thickness of the cell wall and cell composition [50,51].

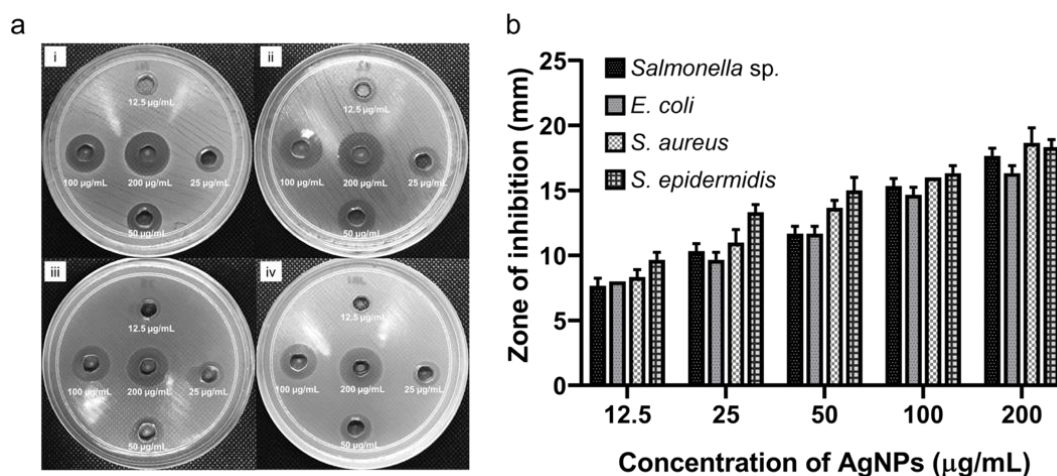


Figure 7. (a) Antibacterial activity of biosynthesized AgNPs using agar well diffusion method against (i) *S. aureus*, (ii) *S. epidermidis*, (iii) *E. coli*, and (iv) *Salmonella* sp. (b) Zone of inhibition of biosynthesized AgNPs at different concentrations. Each value represents the mean \pm SD of three replicates.

Although the efficacy of AgNPs as an antibacterial agent has been demonstrated, the exact mechanisms behind the operation have not been completely deciphered. The most common mechanism involved is the release of Ag^+ from the AgNPs. AgNPs act in the same way as silver salt; however, the bactericidal activity of AgNPs and silver salt are at nanomolar and micromolar concentrations, respectively [52]. It is well documented that the Ag^+ released from AgNPs may interact with the surface of the bacterial cell, particularly with functional groups of protein resulting in their deactivation [6]. Furthermore, the potential antibacterial activity of AgNPs may be attributed to the physical contact of NPs via electrostatic forces with the bacterial cell wall and leads to the penetration of NPs into the cells, which could be toxic to biomolecules of the cell [53]. A recent study has revealed that the contact

between AgNPs and *E. coli* cell membrane for a few minutes led to the disruption of cells, as visualized by TEM [54]. Moreover, it was also suggested that AgNPs exert their antibacterial activity through the inactivation of the respiratory membrane chain of bacteria, which resulted in the generation of excess Reactive oxygen species (ROS) and accumulation in the cell, leading to cell death [55]. It should be noted that the ROS are generated intracellularly during the mitochondrial oxidative phosphorylation of bacterial cell.

Researchers also suggested that the most prominent antibacterial mechanisms are related to the size of NPs. Morones et al. [56] reported that the smaller size of AgNPs has a greater bactericidal effect than the larger ones due to the large surface area of NPs, which increases the surface reactivity. For instance, the smallest size of NPs releases a high concentration of Ag^+ , while the biggest NPs release the lowest concentration of Ag^+ [57]. Lu et al. [58] demonstrated that different sizes of AgNPs (5, 15, and 55 nm) exhibited different inhibition rates against oral pathogenic bacteria. In their study, the AgNPs of 5 nm size presented greater antibacterial activity compared to the AgNPs of 15 and 55 nm sizes due to their greater surface area. Similarly, AgNPs with the size of 10 nm completely inhibited pathogenic bacteria at the lowest minimum inhibitory concentration (MIC) of 1.0 $\mu\text{g}/\text{mL}$, whereas at the size of 90 nm exhibited higher MIC of 11.5 $\mu\text{g}/\text{mL}$ [59]. In our study, it can be postulated that the significant inhibitory effect of biosynthesized AgNPs against tested pathogens is due to its smaller particle size.

3.7. Antioxidant Activity of Biosynthesized AgNPs

In this study, the in vitro antioxidant activity of biosynthesized AgNPs was determined using DPPH radical scavenging assay. DPPH has been widely used to measure the antioxidant activity due to its stable compound. Figure 8 shows the effect of different concentrations of AgNPs on DPPH radical antioxidant activity. Our results revealed that the biosynthesized AgNPs exhibited a moderate antioxidant activity compared to ascorbic acid, which shows greater activity. In the case of DPPH assay, the principle of the antioxidant properties is attributable to the electron-donating behavior of the AgNPs to the odd electron in the DPPH solution, and consequently to a decrease in the intensity of $n \rightarrow \pi^*$ transition at 517 nm (color changes from deep purple to pale yellow) [60], indicating the effect of antioxidant activity. In addition, AgNPs are reported to possess intrinsic antioxidant properties associated with their surface properties. Metal NPs (gold, silver, and palladium) have been reported to exhibit catalase-mimicking behavior by decomposing H_2O_2 to H_2O and O_2 at neutral and basic pH values [61]. Nevertheless, the different concentrations of biosynthesized AgNPs (250, 500, and 1000 $\mu\text{g}/\text{mL}$) have no direct influence on the scavenging activity, which may be attributed to the protein or biological compound from *L. plantarum* TA4 that covered or layered the surface of AgNPs and interfere with the reactivity of NPs. This phenomenon was also observed by Das et al. [62], who employed fruit extract for the biosynthesis of AgNPs. They postulated that several functional groups in the fruit act as a capping agent and covered the NPs, which resulted in moderate antioxidant activity.

Moreover, it was found that the elevated AgNPs concentration reduced the solubility of NPs, which explained the reduction in scavenging activity at concentration of 500 and 1000 $\mu\text{g}/\text{mL}$. Furthermore, it might also be due to a lack of DPPH content at higher concentrations. Likewise, Kumar et al. [63] and Moghaddam et al. [64] have also reported that the high concentration of NPs does not correlate with their scavenging activity. On the contrary, Khorrami et al. [65] reported that the biosynthesized AgNPs employing walnut green husk extract exhibited improved antioxidant activity with increased concentration. They suggested that the biologically active compounds from the extract, such as flavonoids, ellagic acid, and valeric acid bound on the NPs, improved the antioxidant properties of AgNPs. Similarly, *Lenzites betulina*-capped AgNPs were also reported to promote stable radical reduction [66]. Therefore, the synthesis of AgNPs using biological substances influenced the biological and chemical activity through the attachment of biologically active compounds on the surface of NPs.

In the present study, the biological compound from *L. plantarum* TA4 did not promote the antioxidant activity but acted as a stabilizing agent.

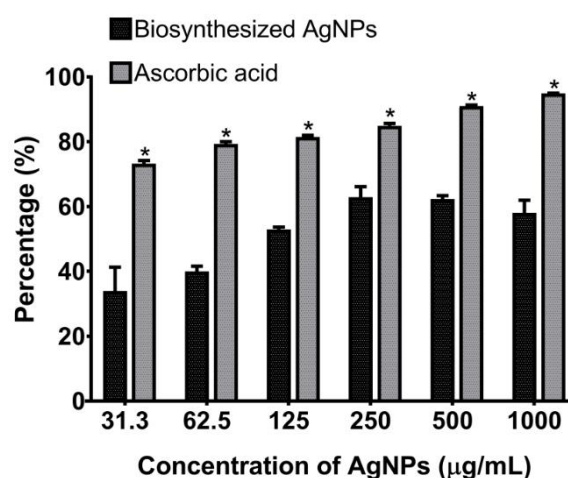


Figure 8. Antioxidant activity of biosynthesized AgNPs. Ascorbic acid was used as a positive control. Each value represents the mean \pm SD of three replicates. * $p < 0.05$.

4. Conclusions

In conclusion, this study demonstrated the production of AgNPs employing cell biomass of *L. plantarum* TA4. The *L. plantarum* TA4 was found to have silver metal tolerance ability at the concentration of 2 mM and simultaneously produced AgNPs. The AgNPs were spherical, with an average particle size of 14.0 ± 4.7 nm with monodispersed NPs. Based on the SEM-EDX analysis, the formation of AgNPs was found distributed on the cell membrane, indicating the involvement of biomolecules and functional groups present on the cell surface to initiate the biosynthesis of AgNPs. Moreover, the FTIR analysis detected the presence of hydroxyl, carboxyl, and protein on the surface of AgNPs, which confirmed the involvement of these functional groups in the reduction and stabilization process. Furthermore, biosynthesized AgNPs exhibited considerable antibacterial activity against Gram-negative and Gram-positive pathogens in a concentration-dependent manner, indicating the potential application as an antibacterial agent. Moreover, the in vitro antioxidant activity of AgNPs demonstrated moderate radical scavenging activity on DPPH. The findings in our study highlight the sustainable and low-cost approach in the development of AgNPs, which can be the best alternative to the conventional method.

Author Contributions: Conceptualization, H.M.Y. and N.A.R.; data curation, H.M.Y.; formal analysis, H.M.Y., N.A.R., R.M., and U.H.Z.; funding acquisition, N.A.R.; investigation, H.M.Y.; methodology, H.M.Y.; project administration, N.A.R.; resources, N.A.R.; software, H.M.Y.; supervision, N.A.R., R.M., and U.H.Z.; validation, N.A.R. and R.M.; visualization, H.M.Y.; writing—original draft, H.M.Y. and N.A.R.; and writing—review and editing, N.A.R., R.M., and U.H.Z. All authors have read and agreed to the published version of the manuscript.

Funding: This research received no external funding.

Acknowledgments: The authors would like to thank Universiti Putra Malaysia for the financial support given.

Conflicts of Interest: The authors declare no conflict of interest.

References

1. Firdhouse, M.J.; Lalitha, P. Biosynthesis of Silver Nanoparticles and Its Applications. *J. Nanotechnol.* **2015**, *2015*, 1–18. [[CrossRef](#)]
2. Lee, S.; Jun, B.-H. Silver Nanoparticles: Synthesis and Application for Nanomedicine. *Int. J. Mol. Sci.* **2019**, *20*, 865. [[CrossRef](#)] [[PubMed](#)]

3. Yan, J.; Abdelgawad, A.M.; El-Naggar, M.E.; Rojas, O.J. Antibacterial activity of silver nanoparticles synthesized In-situ by solution spraying onto cellulose. *Carbohydr. Polym.* **2016**, *147*, 500–508. [[CrossRef](#)] [[PubMed](#)]
4. Paladini, F.; Pollini, M. Antimicrobial Silver Nanoparticles for Wound Healing Application: Progress and Future Trends. *Materials* **2019**, *12*, 2540. [[CrossRef](#)] [[PubMed](#)]
5. Simbine, E.O.; Rodrigues, L.; Da, C.; Lapa-Guimarães, J.; Kamimura, E.S.; Corassin, C.H.; Oliveira, C.A.F.D. Application of silver nanoparticles in food packages: A review. *Food Sci. Technol.* **2019**, *39*, 793–802. [[CrossRef](#)]
6. Dakal, T.C.; Kumar, A.; Majumdar, R.S.; Yadav, V. Mechanistic Basis of Antimicrobial Actions of Silver Nanoparticles. *Front. Microbiol.* **2016**, *7*, 1831. [[CrossRef](#)]
7. Durán, N.; Marcato, P.D.; Durán, M.; Yadav, A.; Gade, A.; Rai, M. Mechanistic aspects in the biogenic synthesis of extracellular metal nanoparticles by peptides, bacteria, fungi, and plants. *Appl. Microbiol. Biotechnol.* **2011**, *90*, 1609–1624. [[CrossRef](#)]
8. Xu, C.; Guo, Y.; Qiao, L.; Ma, L.; Cheng, Y.; Roman, A. Biogenic Synthesis of Novel Functionalized Selenium Nanoparticles by *Lactobacillus casei* ATCC 393 and Its Protective Effects on Intestinal Barrier Dysfunction Caused by Enterotoxigenic *Escherichia coli* K88. *Front. Microbiol.* **2018**, *9*, 1129. [[CrossRef](#)]
9. Markus, J.; Mathiyalagan, R.; Kim, Y.J.; Abbai, R.; Singh, P.; Ahn, S.; Perez, Z.E.J.; Hurh, J.; Yang, D.C. Intracellular synthesis of gold nanoparticles with antioxidant activity by probiotic *Lactobacillus kimchicus* DCY51T isolated from Korean kimchi. *Enzym. Microb. Technol.* **2016**, *95*, 85–93. [[CrossRef](#)]
10. Mohd Yusof, H.; Mohamad, R.; Zaidan, U.H.; Rahman, N.A. Sustainable microbial cell nanofactory for zinc oxide nanoparticles production by zinc-tolerant probiotic *Lactobacillus plantarum* strain TA4. *Microb. Cell Factories* **2020**, *19*, 10. [[CrossRef](#)]
11. Sintubin, L.; De Windt, W.; Dick, J.; Mast, J.; van der Ha, D.; Verstraete, W.; Boon, N. Lactic acid bacteria as reducing and capping agent for the fast and efficient production of silver nanoparticles. *Appl. Microbiol. Biotechnol.* **2009**, *84*, 741–749. [[CrossRef](#)] [[PubMed](#)]
12. Mrvčić, J.; Stanzer, D.; Šolić, E.; Stehlik-Tomas, V. Interaction of lactic acid bacteria with metal ions: Opportunities for improving food safety and quality. *World J. Microbiol. Biotechnol.* **2012**, *28*, 2771–2782. [[CrossRef](#)] [[PubMed](#)]
13. Król, A.; Railean-Plugaru, V.; Pomastowski, P.; Złoch, M.; Buszewski, B. Mechanism study of intracellular zinc oxide nanocomposites formation. *Colloids Surf. A Physicochem. Eng. Asp.* **2018**, *553*, 349–358. [[CrossRef](#)]
14. Jain, N.; Bhargava, A.; Tarafdar, J.C.; Singh, S.K.; Panwar, J. A biomimetic approach towards synthesis of zinc oxide nanoparticles. *Appl. Microbiol. Biotechnol.* **2013**, *97*, 859–869. [[CrossRef](#)]
15. Bhargava, A.; Jain, N.; Khan, M.A.; Pareek, V.; Dilip, R.V.; Panwar, J. Utilizing metal tolerance potential of soil fungus for efficient synthesis of gold nanoparticles with superior catalytic activity for degradation of rhodamine B. *J. Environ. Manag.* **2016**, *183*, 22–32. [[CrossRef](#)]
16. George Kerry, R.; Patra, J.K.; Gouda, S.; Park, Y.; Shin, H.-S.; Das, G. Benefaction of probiotics for human health: A review. *J. Food Drug Anal.* **2018**, *26*, 927–939. [[CrossRef](#)]
17. Rajesh, S.; Dharanishanthi, V.; Kanna, A.V. Antibacterial mechanism of biogenic silver nanoparticles of *Lactobacillus acidophilus*. *J. Exp. Nanosci.* **2015**, *10*, 1143–1152. [[CrossRef](#)]
18. Chaudhari, P.R.; Masurkar, S.A.; Shidore, V.B.; Kamble, S.P. Antimicrobial activity of extracellularly synthesized silver nanoparticles using *Lactobacillus* species obtained from VIZYLAC capsule. *J. Appl. Pharm. Sci.* **2012**, *2*, 25.
19. Dakhil, A.S. Biosynthesis of silver nanoparticle (AgNPs) using *Lactobacillus* and their effects on oxidative stress biomarkers in rats. *J. King Saud Univ.-Sci.* **2017**, *29*, 462–467. [[CrossRef](#)]
20. Viorica, R.-P.; Pawel, P.; Kinga, M.; Michal, Z.; Katarzyna, R.; Boguslaw, B. *Lactococcus lactis* as a safe and inexpensive source of bioactive silver composites. *Appl. Microbiol. Biotechnol.* **2017**, *101*, 7141–7153. [[CrossRef](#)]
21. Das, V.L.; Thomas, R.; Varghese, R.T.; Soniya, E.V.; Mathew, J.; Radhakrishnan, E.K. Extracellular synthesis of silver nanoparticles by the *Bacillus* strain CS 11 isolated from industrialized area. *3 Biotech* **2014**, *4*, 121–126. [[CrossRef](#)] [[PubMed](#)]
22. Presentato, A.; Piacenza, E.; Anikovskiy, M.; Cappelletti, M.; Zannoni, D.; Turner, R.J. Biosynthesis of selenium-nanoparticles and -nanorods as a product of selenite bioconversion by the aerobic bacterium *Rhodococcus aetherivorans* BCP1. *New Biotechnol.* **2018**, *41*, 1–8. [[CrossRef](#)] [[PubMed](#)]

23. Thomas, R.; Janardhanan, A.; Varghese, R.T.; Soniya, E.V.; Mathew, J.; Radhakrishnan, E.K. Antibacterial properties of silver nanoparticles synthesized by marine *Ochrobactrum* sp. *Braz. J. Microbiol.* **2014**, *45*, 1221–1227. [[CrossRef](#)] [[PubMed](#)]
24. Safawo, T.; Sandeep, B.; Pola, S.; Tadesse, A. Synthesis and characterization of zinc oxide nanoparticles using tuber extract of anchote (*Coccinia abyssinica* (Lam.) Cong.) for antimicrobial and antioxidant activity assessment. *OpenNano* **2018**, *3*, 56–63. [[CrossRef](#)]
25. Mohd Yusof, H.; Mohamad, R.; Zaidan, U.H.; Abdul Rahman, N. Microbial synthesis of zinc oxide nanoparticles and their potential application as an antimicrobial agent and a feed supplement in animal industry: A review. *J. Anim. Sci. Biotechnol.* **2019**, *10*, 1–22. [[CrossRef](#)]
26. Zonaro, E.; Piacenza, E.; Presentato, A.; Monti, F.; Dell'Anna, R.; Lampis, S.; Vallini, G. *Ochrobactrum* sp. MPV1 from a dump of roasted pyrites can be exploited as bacterial catalyst for the biogenesis of selenium and tellurium nanoparticles. *Microb. Cell Factories* **2017**, *16*, 215. [[CrossRef](#)]
27. Giller, K.E.; Witter, E.; McGrath, S.P. Heavy metals and soil microbes. *Soil Biol. Biochem.* **2009**, *41*, 2031–2037. [[CrossRef](#)]
28. Klaus, T.; Joerger, R.; Olsson, E.; Granqvist, C.-G. Silver-based crystalline nanoparticles, microbially fabricated. *Proc. Natl. Acad. Sci. USA* **1999**, *96*, 13611–13614. [[CrossRef](#)]
29. Irvani, S. Bacteria in Nanoparticle Synthesis: Current Status and Future Prospects. *Int. Sch. Res. Not.* **2014**, *2014*, 1–18. [[CrossRef](#)]
30. Kamika, I.; Momba, M.N.B. Assessing the resistance and bioremediation ability of selected bacterial and protozoan species to heavy metals in metal-rich industrial wastewater. *BMC Microbiol.* **2013**, *13*, 28. [[CrossRef](#)]
31. Mohanta, Y.K.; Panda, S.K.; Bastia, A.K.; Mohanta, T.K. Biosynthesis of Silver Nanoparticles from *Protium serratum* and Investigation of their Potential Impacts on Food Safety and Control. *Front. Microbiol.* **2017**, *8*, 826. [[CrossRef](#)] [[PubMed](#)]
32. Ibrahim, E.; Fouad, H.; Zhang, M.; Zhang, Y.; Qiu, W.; Yan, C.; Li, B.; Mo, J.; Chen, J. Biosynthesis of silver nanoparticles using endophytic bacteria and their role in inhibition of rice pathogenic bacteria and plant growth promotion. *RSC Adv.* **2019**, *9*, 29293–29299. [[CrossRef](#)]
33. El-Shanshoury, A.E.-R.R.; ElSilk, S.E.; Ebeid, M.E. Extracellular Biosynthesis of Silver Nanoparticles Using *Escherichia coli* ATCC 8739, *Bacillus subtilis* ATCC 6633, and *Streptococcus thermophilus* ESh1 and Their Antimicrobial Activities. *ISRN Nanotechnol.* **2011**, *2011*, 1–7. [[CrossRef](#)]
34. Nanda, A.; Saravanan, M. Biosynthesis of silver nanoparticles from *Staphylococcus aureus* and its antimicrobial activity against MRSA and MRSE. *Nanomed. Nanotechnol. Biol. Med.* **2009**, *5*, 452–456. [[CrossRef](#)] [[PubMed](#)]
35. Garmasheva, I.; Kovalenko, N.; Voychuk, S.; Ostapchuk, A.; Livins'ka, O.; Oleschenko, L. *Lactobacillus* species mediated synthesis of silver nanoparticles and their antibacterial activity against opportunistic pathogens in vitro. *BioImpacts* **2016**, *6*, 219–223. [[CrossRef](#)]
36. Saravanan, M.; Nanda, A.; Kingsley, S.J. *Lactobacillus delbrueckii* mediated synthesis of silver nanoparticles and their evaluation of antibacterial efficacy against MDR clinical pathogens. In Proceedings of the International Conference on Nanoscience, Engineering and Technology (ICONSET 2011), Chennai, India, 28–30 November 2011; pp. 386–390.
37. Matei, A.; Matei, S.; Matei, G.-M.; Cogălniceanu, G.; Cornea, C.P. Biosynthesis of silver nanoparticles mediated by culture filtrate of lactic acid bacteria, characterization and antifungal activity. *EuroBiotech J.* **2020**, *4*, 97–103. [[CrossRef](#)]
38. Dhoondia, Z.H.; Chakraborty, H. *Lactobacillus* Mediated Synthesis of Silver Oxide Nanoparticles. *Nanomater. Nanotechnol.* **2012**, *2*, 15. [[CrossRef](#)]
39. Anil Kumar, S.; Abyaneh, M.K.; Gosavi, S.W.; Kulkarni, S.K.; Pasricha, R.; Ahmad, A.; Khan, M.I. Nitrate reductase-mediated synthesis of silver nanoparticles from AgNO₃. *Biotechnol. Lett.* **2007**, *29*, 439–445. [[CrossRef](#)]
40. Samuel, M.S.; Jose, S.; Selvarajan, E.; Mathimani, T.; Pugazhendhi, A. Biosynthesized silver nanoparticles using *Bacillus amyloliquefaciens*; Application for cytotoxicity effect on A549 cell line and photocatalytic degradation of p-nitrophenol. *J. Photochem. Photobiol. B Biol.* **2020**, *202*, 111642. [[CrossRef](#)]
41. Wang, Y.; Shu, X.; Hou, J.; Lu, W.; Zhao, W.; Huang, S.; Wu, L. Selenium Nanoparticle Synthesized by *Proteus mirabilis* YC801: An Efficacious Pathway for Selenite Biotransformation and Detoxification. *Int. J. Mol. Sci.* **2018**, *19*, 3809. [[CrossRef](#)]

42. Chapot-Chartier, M.-P.; Kulakauskas, S. Cell wall structure and function in lactic acid bacteria. *Microb. Cell Factories* **2014**, *13*, S9. [[CrossRef](#)]
43. Omran, B.A.; Nassar, H.N.; Younis, S.A.; Fatthallah, N.A.; Hamdy, A.; El-Shatoury, E.H.; El-Gendy, N.S. Physiochemical properties of *Trichoderma longibrachiatum* DSMZ 16517-synthesized silver nanoparticles for the mitigation of halotolerant sulphate-reducing bacteria. *J. Appl. Microbiol.* **2019**, *126*, 138–154. [[CrossRef](#)]
44. Tomaszewska, E.; Soliwoda, K.; Kadziola, K.; Tkacz-Szczesna, B.; Celichowski, G.; Cichowski, M.; Szmaja, W.; Grobelny, J. Detection Limits of DLS and UV-Vis Spectroscopy in Characterization of Polydisperse Nanoparticles Colloids. *J. Nanomater.* **2013**, *2013*, 1–10. [[CrossRef](#)]
45. Hamouda, R.A.; Hussein, M.H.; Abo-elmagd, R.A.; Bawazir, S.S. Synthesis and biological characterization of silver nanoparticles derived from the cyanobacterium *Oscillatoria limnetica*. *Sci. Rep.* **2019**, *9*, 13071. [[CrossRef](#)] [[PubMed](#)]
46. Moreno-Martin, G.; Pescuma, M.; Pérez-Corona, T.; Mozzi, F.; Madrid, Y. Determination of size and mass-and number-based concentration of biogenic SeNPs synthesized by lactic acid bacteria by using a multimethod approach. *Anal. Chim. Acta* **2017**, *992*, 34–41. [[CrossRef](#)] [[PubMed](#)]
47. Nair, B.; Pradeep, T. Coalescence of Nanoclusters and Formation of Submicron Crystallites Assisted by *Lactobacillus* Strains. *Cryst. Growth Des.* **2002**, *2*, 293–298. [[CrossRef](#)]
48. Butler, K.S.; Peeler, D.J.; Casey, B.J.; Dair, B.J.; Elespuru, R.K. Silver nanoparticles: Correlating nanoparticle size and cellular uptake with genotoxicity. *Mutagenesis* **2015**, *30*, 577–591. [[CrossRef](#)] [[PubMed](#)]
49. Gosens, I.; Post, J.A.; de la Fonteyne, L.J.J.; Jansen, E.H.J.M.; Geus, J.W.; Cassee, F.R.; de Jong, W.H. Impact of agglomeration state of nano- and submicron sized gold particles on pulmonary inflammation. *Part. Fibre Toxicol.* **2010**, *7*, 1–11. [[CrossRef](#)]
50. Bilal, M.; Rasheed, T.; Iqbal, H.M.N.; Li, C.; Hu, H.; Zhang, X. Development of silver nanoparticles loaded chitosan-alginate constructs with biomedical potentialities. *Int. J. Biol. Macromol.* **2017**, *105*, 393–400. [[CrossRef](#)]
51. Priyadarshini, S.; Gopinath, V.; Meera Priyadharsshini, N.; MubarakAli, D.; Velusamy, P. Synthesis of anisotropic silver nanoparticles using novel strain, *Bacillus flexus* and its biomedical application. *Colloids Surf. B Biointerfaces* **2013**, *102*, 232–237. [[CrossRef](#)]
52. Yan, X.; He, B.; Liu, L.; Qu, G.; Shi, J.; Hu, L.; Jiang, G. Antibacterial mechanism of silver nanoparticles in: *Pseudomonas aeruginosa*: Proteomics approach. *Metallomics* **2018**, *10*, 557–564. [[CrossRef](#)] [[PubMed](#)]
53. Seil, J.T.; Webster, T.J. Antimicrobial applications of nanotechnology: Methods and literature. *Int. J. Nanomed.* **2012**, *7*, 2767–2781.
54. Raffi, M.; Hussain, F.; Bhatti, T.M.; Akhter, J.I.; Hameed, A.; Hasan, M.M. Antibacterial characterization of silver nanoparticles against *E.coli* ATCC-15224. *J. Mater. Sci. Technol.* **2008**, *24*, 192–196.
55. Quinteros, M.A.; Cano Aristizábal, V.; Dalmasso, P.R.; Paraje, M.G.; Páez, P.L. Oxidative stress generation of silver nanoparticles in three bacterial genera and its relationship with the antimicrobial activity. *Toxicol. Vitro.* **2016**, *36*, 216–223. [[CrossRef](#)]
56. Morones, J.R.; Elechiguerra, J.L.; Camacho, A.; Holt, K.; Kouri, J.B.; Ramírez, J.T.; Yacaman, M.J. The bactericidal effect of silver nanoparticles. *Nanotechnology* **2005**, *16*, 2346–2353. [[CrossRef](#)] [[PubMed](#)]
57. Qing, Y.; Cheng, L.; Li, R.; Liu, G.; Zhang, Y.; Tang, X.; Wang, J.; Liu, H.; Qin, Y. Potential antibacterial mechanism of silver nanoparticles and the optimization of orthopedic implants by advanced modification technologies. *Int. J. Nanomed.* **2018**, *12*, 3311. [[CrossRef](#)]
58. Lu, Z.; Rong, K.; Li, J.; Yang, H.; Chen, R. Size-dependent antibacterial activities of silver nanoparticles against oral anaerobic pathogenic bacteria. *J. Mater. Sci. Mater. Med.* **2013**, *24*, 1465–1471. [[CrossRef](#)]
59. Dong, Y.; Zhu, H.; Shen, Y.; Zhang, W.; Zhang, L. Antibacterial activity of silver nanoparticles of different particle size against *Vibrio Natriegens*. *PLoS ONE* **2019**, *14*, e0222322. [[CrossRef](#)]
60. Das, D.; Nath, B.C.; Phukon, P.; Kalita, A.; Dolui, S.K. Synthesis of ZnO nanoparticles and evaluation of antioxidant and cytotoxic activity. *Colloids Surf. B Biointerfaces* **2013**, *111*, 556–560. [[CrossRef](#)]
61. Valgimigli, L.; Baschieri, A.; Amorati, R. Antioxidant activity of nanomaterials. *J. Mater. Chem. B* **2018**, *6*, 2036–2051. [[CrossRef](#)]
62. Das, G.; Patra, J.K.; Debnath, T.; Ansari, A.; Shin, H.-S. Investigation of antioxidant, antibacterial, antidiabetic, and cytotoxicity potential of silver nanoparticles synthesized using the outer peel extract of *Ananas comosus* (L.). *PLoS ONE* **2019**, *14*, e0220950. [[CrossRef](#)]

63. Kumar, B.; Smita, K.; Seqqat, R.; Benalcazar, K.; Grijalva, M.; Cumbal, L. In vitro evaluation of silver nanoparticles cytotoxicity on Hepatic cancer (Hep-G2) cell line and their antioxidant activity: Green approach for fabrication and application. *J. Photochem. Photobiol. B Biol.* **2016**, *159*, 8–13. [[CrossRef](#)] [[PubMed](#)]
64. Moghaddam, A.B.; Moniri, M.; Azizi, S.; Rahim, R.A.; Ariff, A.B.; Saad, W.Z.; Namvar, F.; Navaderi, M.; Mohamad, R. Biosynthesis of ZnO nanoparticles by a new *Pichia kudriavzevii* yeast strain and evaluation of their antimicrobial and antioxidant activities. *Molecules* **2017**, *22*, 872. [[CrossRef](#)] [[PubMed](#)]
65. Khorrami, S.; Zarrabi, A.; Khaleghi, M.; Danaei, M.; Mozafari, M. Selective cytotoxicity of green synthesized silver nanoparticles against the MCF-7 tumor cell line and their enhanced antioxidant and antimicrobial properties. *Int. J. Nanomed.* **2018**, *13*, 8013–8024. [[CrossRef](#)] [[PubMed](#)]
66. Sytu, M.R.C.; Camacho, D.H. Green Synthesis of Silver Nanoparticles (AgNPs) from *Lenzites betulina* and the Potential Synergistic Effect of AgNP and Capping Biomolecules in Enhancing Antioxidant Activity. *Bionanoscience* **2018**, *8*, 835–844. [[CrossRef](#)]



© 2020 by the authors. Licensee MDPI, Basel, Switzerland. This article is an open access article distributed under the terms and conditions of the Creative Commons Attribution (CC BY) license (<http://creativecommons.org/licenses/by/4.0/>).